

# Generic Contrast Agents

Our portfolio is growing to serve you better. Now you have a *choice*.



[VIEW CATALOG](#)

# AJNR

## High-resolution MR imaging of the cadaveric human spinal cord: normal anatomy.

M D Solsberg, C Lemaire, L Resch and D G Potts

*AJNR Am J Neuroradiol* 1990, 11 (1) 3-7

<http://www.ajnr.org/content/11/1/3>

This information is current as of May 9, 2025.

# High-Resolution MR Imaging of the Cadaveric Human Spinal Cord: Normal Anatomy

M. D. Solsberg<sup>1</sup>  
 C. Lemaire<sup>1,2</sup>  
 L. Resch<sup>3</sup>  
 D. G. Potts<sup>1</sup>

The purpose of this study was to demonstrate the regional MR anatomy of a normal human spinal cord under near optimal conditions. A spinal cord and meninges were excised and segments from the cervical (C6), thoracic (T6), lumbar (L3), and sacral/cauda equina regions were examined on a 2-T MR system. By using a 2.5 × 2.0 cm solenoid coil and a multislice spin-echo sequence, we achieved a resolution of 58 μm in the readout direction and 117 μm in the phase-encode direction. Histological sections corresponding to the areas imaged by MR were retained and treated with stains that demonstrated the distributions of collagen (hematoxylin, phloxine, saffron), myelin (Luxol fast blue/H and E), or neuritic processes (Bielschowsky's). Subarachnoid, vascular, white matter, and gray matter structures were demonstrated by MR and light microscopy. The resulting MR images and photomicrographs were correlated. Different signal intensities were observed in the gracile and cuneate fasciculi, and these differences were similar to the pattern seen with the myelin stain. Decreased signal intensity was present in the region of the spinocerebellar tracts.

The anatomic detail demonstrated by this study was clearly superior to that shown by clinical MR examinations.

*AJNR* 11:3-7, January/February 1990

Because MR imaging of the human spinal cord demonstrates clearly the gray and white matter structures [1-5], this technique is useful for diagnosing various cord abnormalities, such as syringomyelia, intramedullary tumors, cord atrophy demyelination, cord cysts, and vascular malformations. In spite of its obvious diagnostic advantages for cord studies, MR has significant limitations. For example, MR images of patients with clear clinical manifestations of spinal cord disease can fail to demonstrate any abnormality.

Carvlin et al. [6] have used high-resolution MR imaging to study fresh and fixed human and rat cord specimens and have published images showing anatomic detail that is greatly improved over clinical studies.

The purposes of this study were to obtain high-resolution MR images of the human spinal cord at various levels under near ideal conditions and to compare these images with corresponding histological sections and standard anatomic descriptions.

## Materials and Methods

The spinal cord of an adult male with no history suggestive of neurologic disease was excised during a postmortem examination. The specimen included the entire cord, cauda equina, and dura excised from the foramen magnum to the sacrum. Immediately after removal, the specimen was placed in a 10% formalin solution for 7 days.

After fixation, 3-cm lengths of cord and dura were removed from the cervical (center of segment at the C6 nerve root), thoracic (T6), lumbar (L3), and sacral/cauda equina (end of the spinal cord) regions. The rostral end of each specimen was identified.

Received April 11, 1989; revision requested May 30, 1989; revision received June 12, 1989; accepted September 20, 1989.

Presented at the annual meeting of the American Society of Neuroradiology, Orlando, March 1989.

<sup>1</sup> Department of Radiology, University of Toronto, Toronto Western Hospital, Magnetic Resonance Laboratory, Toronto, Ontario, Canada M5T 2S8. Address reprint requests to M. D. Solsberg, 1177 Yonge St., Suite 704, Toronto, Ontario, Canada M4T 2Y4.

<sup>2</sup> Department of Physics, University of Toronto, Toronto Western Hospital, Toronto, Ontario, Canada M5T 2S8.

<sup>3</sup> Department of Neuropathology, University of Toronto, Toronto Western Hospital, Toronto, Ontario, Canada M5T 2S8.

0195-6108/90/1101-003

© American Society of Neuroradiology

The samples were placed inside a closely fitting plastic cylinder and centered in a five-turn 12-gauge copper wire solenoid coil, which was 2.5 cm in length and 2.0 cm in diameter. The quality factor of the unloaded coil, as determined by resonance absorption curves, was 200 at 85 MHz. The unloaded/loaded ratio of the 180° pulse lengths was used as a measure of the relative signal-to-noise ratio [7]. This ratio was approximately 2:3 for all samples. The specimens were examined in a General Electric (Fremont, CA) 2-T CSI system. After equilibration, the system was tuned and shimmed in the usual fashion.

Images were obtained with a multislice spin-echo sequence. For each sample a sagittal image was acquired and the rostral edge of the specimen was determined as a reference plane. Nine transverse images of 1-mm slice thickness were obtained for each sample. The resolution achieved, prior to zero filling, was 58  $\mu\text{m}$  in the readout direction and 117  $\mu\text{m}$  in the phase-encode direction. Improvements in contrast between gray and white matter structures were achieved by varying the TEs and TRs of the imaging sequences and comparing the results. Typically, the (TR/TE/excitation) values were 800/40/8 for maximum differentiation of gray and white matter cord structures.

The spinal cord segments were then submitted for histological processing. Specimens were embedded in paraffin and then sectioned with a microtome. The slices were 5  $\mu\text{m}$  thick.

For each spinal cord segment, histological sections were retained from the areas corresponding to the MR images. Individual sections were stained with one of the following three stains. Hematoxylin, phloxine, saffron stain showed the cellular and collagen distribution. Luxol fast blue/H and E stain showed myelin-containing structures. Bielschowsky's stain showed the distribution of axons and neuritic processes.

The sections were then examined by light microscopy and the resulting photomicrographs were compared with the corresponding MR images and anatomic descriptions [8-10].

## Results

### *Subarachnoid Structures and Dura Mater*

The dura mater and pia/arachnoid mater are demonstrated best in the MR image at C6 (Fig. 1A). The dentate ligaments are not clearly demonstrated in either the MR images or photomicrographs because the dura mater is collapsed in the specimens.

The bilateral dorsal nerve roots are shown more completely in the 1-mm-thick MR images than in the 5- $\mu\text{m}$  histological sections (Figs. 1B and 1C). Ventral nerve rootlets are not seen in the subarachnoid space.

The spinal nerve roots also are seen in the MR images and photomicrographs at other levels (Figs. 2-5). They are particularly well demonstrated in the sacral/cauda equina cord segment images.

The anterior spinal artery is visible as an area of low signal intensity in the MR images and corresponding photomicrographs of the cervical, thoracic, and sacral cord segments. The anterior spinal artery is seen in the superficial portion of the ventral median fissure. The smaller and thinner walled anterior spinal veins and sulcal vessels are not visible in the MR images; however, the MR images do show branches of the anterior spinal veins leaving the anterior gray horns in the thoracic, lumbar, and sacral/cauda equina segments.

The posterior spinal vessels are well demonstrated in the MR images and photomicrographs of the thoracic, lumbar, and sacral/cauda equina regions. Noted also are the posterolateral spinal vein and its branches. The branches of the posterior spinal artery are present in the MR image of the thoracic cord segment.

The cord topography is displayed in the MR images and photomicrographs: The prominent ventral median fissure is present in the midline anteriorly; on the posterior surface, the smaller dorsal median sulcus is present; the dorsolateral sulci lie adjacent to the dorsal nerve roots; and the dorsal intermediate sulci separate the gracile and cuneate fasciculi. The depths of the dorsal intermediate, dorsal median, and dorsolateral sulci are more clearly defined in the MR images than in the photomicrographs, a fact that is attributable to the shearing, shrinkage, and compression of the cord segments during the cutting and embedding process of histological preparation for light microscopy.

### *White Matter*

The white matter of the cord is divided into three funiculi bilaterally. The anterior funiculus lies between the ventral median fissure and the area where the ventral nerve rootlets exit the cord. The lateral funiculus is between the dorsal and ventral spinal nerve roots. The posterior funiculus is between the dorsal median sulcus and the dorsolateral fasciculus and dorsal horns.

In the MR images, the posterior funiculi show differential intensity in the gracile and cuneate fasciculi in the cervical and thoracic cord segments. A higher-intensity signal is present in the fasciculus gracile. Differential uptake of stain was not noted on the hematoxylin, phloxine, saffron preparations. However, in the Luxol fast blue/H and E prepared light microscopy specimens a similar staining pattern was present. Further histochemical and MR correlation will be required to determine if this signal distribution is caused by differences in myelination.

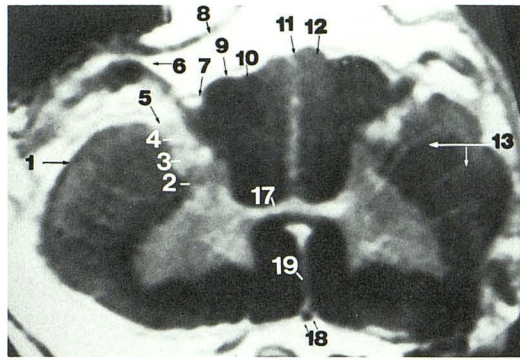
A low-intensity rim is seen in the lateral funiculi in the cervical and thoracic MR images. This area corresponds to the regions of the dorsal and ventral spinocerebellar tracts.

### *Gray Matter*

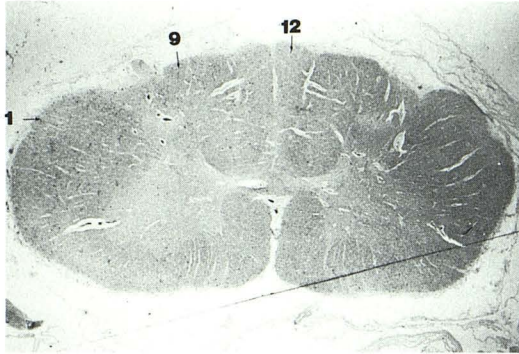
The dorsolateral fasciculus of Lissauer is seen in a position superficial to the underlying substantia gelatinosa. The dorsal funicular gray (nucleus proprius cornu dorsalis) appears as a region of decreased intensity between the substantia gelatinosa and the centrally located gray matter.

In the MR images of the thoracic cord segment, bilateral oblong structures are seen in the region of Clarke's nucleus (nucleus dorsalis), which is located in the middle third of the dorsal central gray matter. This area was apparent in all MR images of the thoracic cord segment, but was not evident on the corresponding photomicrographs.

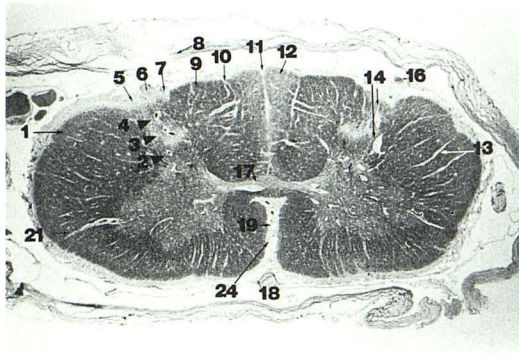
Examination of the sacral cord segments revealed peculiar ringlike structures bilaterally in the region of the lateral motor



A



B



C

## Key for Figures 1-5

1. Location of dorsal and ventral spinocerebellar tracts
2. Dorsal funicular gray
3. Substantia gelatinosa
4. Dorsolateral fasciculus (of Lissauer)
5. Dorsolateral sulcus
6. Dorsal nerve root
7. Pia/arachnoid layers
8. Dura mater
9. Cuneate fasciculus
10. Dorsal intermediate sulcus
11. Dorsal median sulcus
12. Gracile fasciculus
13. Small vascular markings
14. Posterolateral spinal vein tributaries
15. Posterolateral spinal vein and tributary emerging from cord
16. Posterior spinal artery
17. Gray commissure
18. Anterior spinal artery
19. Ventral median fissure
20. Location of Clarke's nucleus (nucleus proprius)
21. Anterior spinal vein tributaries
22. Posterior spinal vein tributaries
23. Unknown structure in sacral anterior horn
24. Sulcal vein
25. Lateral horn

Fig. 1.—Cervical cord (C6).  
 A, MR image (800/40).  
 B, Histology section; hematoxylin, phloxine, saffron stain.  
 C, Histology section; Luxol fast blue/H and E stain.  
 Dorsal nerve roots (6), superficial cord contours (5, 10, 11, 19), and region of dorsal and ventral spinocerebellar tracts (1) are displayed better by MR. Brighter signal is seen in gracile fasciculus (12) than in cuneate fasciculus (9) in MR study. The appearance of these structures is similar in the Luxol fast blue/H and E (myelin) stained histology specimen. Bright appearance of formalin surrounding the specimen on T1-weighted image (A) results from short T1 relaxation time of formalin 10% solution (2.1 sec at 2 T [20°C]) relative to water (2.9 sec at 2 T).

nuclei. We were unable to correlate this structure with either histology or anatomic references.

### Discussion

Light microscopy of stained histological specimens is the gold standard of anatomic tissue evaluation. The exquisite cellular detail obtained is beyond the limits of present MR imaging technology. Nonetheless, MR imaging of small specimens has several advantages over light microscopy techniques.

Standard histological preparation involves formalin fixation, embedding, cutting, and mounting of the thin specimen slices.

The cutting process obviously prevents direct examination of samples in both the transverse and sagittal planes.

The methods of histological preparation result in shrinkage, compression, distortion, and shearing of the specimen. These artifacts are avoided by the minimal sample preparation necessary for MR. In addition, MR allows for examination or reconstruction of structures in any plane.

The laminar structure of the cord is well suited for transverse plane MR. The medullary anatomy varies slowly along the length of the cord and therefore it is clearly shown in relatively thick slices. A 1-mm slice selection shows the dorsal nerve roots and obliquely oriented structures in the subarachnoid space.

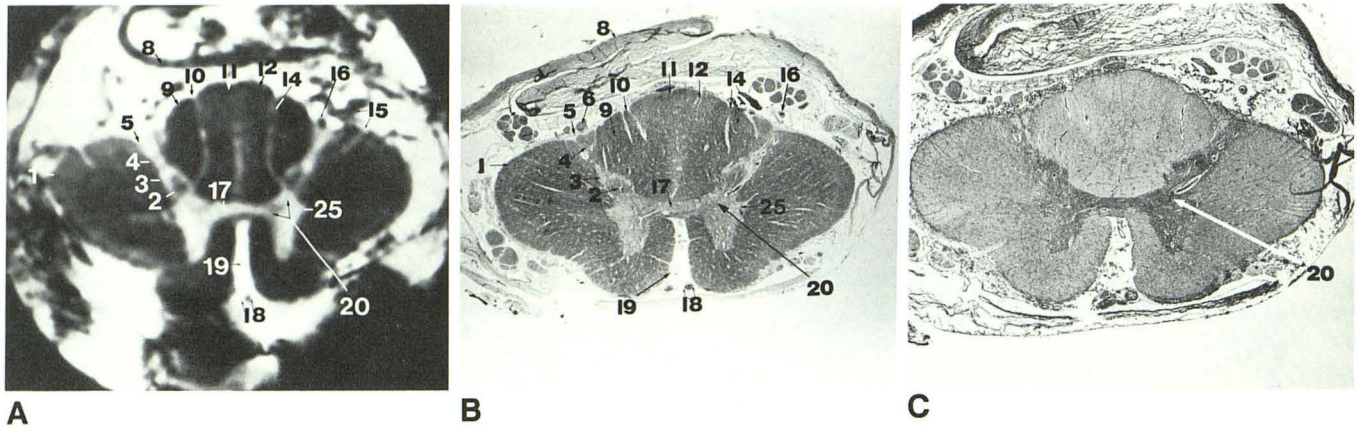


**Fig. 2.—Thoracic cord (T6).**  
**A,** MR image (800/40).  
**B,** Histology section; Luxol fast blue/H and E stain.  
**C,** Histology section; Bielschowsky's stain.  
 Vascular structures (14, 15, 16, 18) are displayed well in the MR image (A). Unknown structure in region of Clarke's nucleus (20) in MR image is not clearly present in histology images.

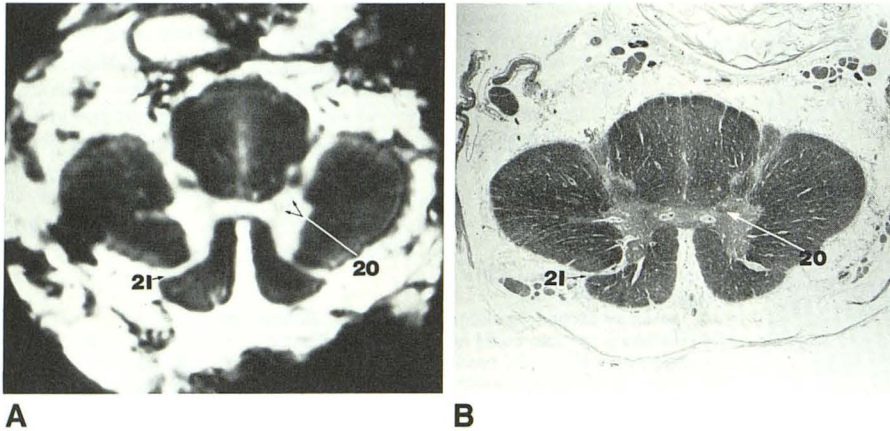


**Fig. 3.—Thoracic cord (T6).**  
**A,** MR image (800/40).  
**B,** Histology section; Luxol fast blue/H and E stain.  
 MR image (A) shows large tributaries of anterior spinal vein (21) emerging from anterior horns. Structures in region of Clarke's nucleus (20) are also demonstrated.

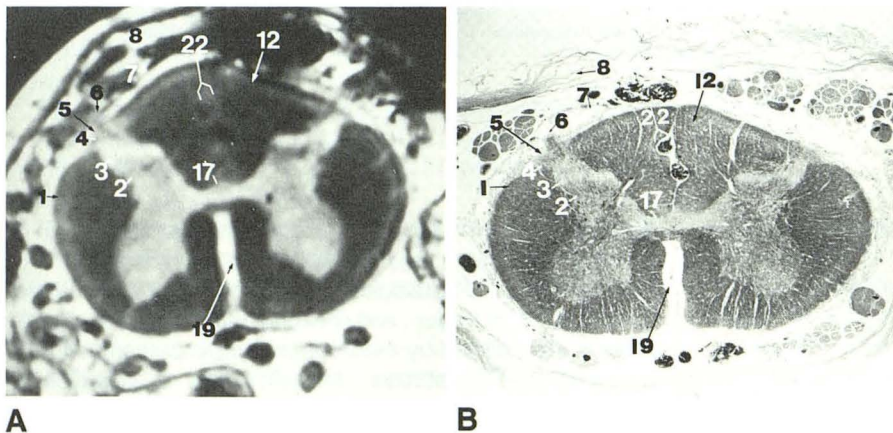


**Fig. 4.—Lumbar cord (L3).**  
**A,** MR image (800/40).  
**B,** Histology section; Luxol fast blue/H and E stain.  
 Note paramedian posterior spinal vein tributaries (22) in both A and B.

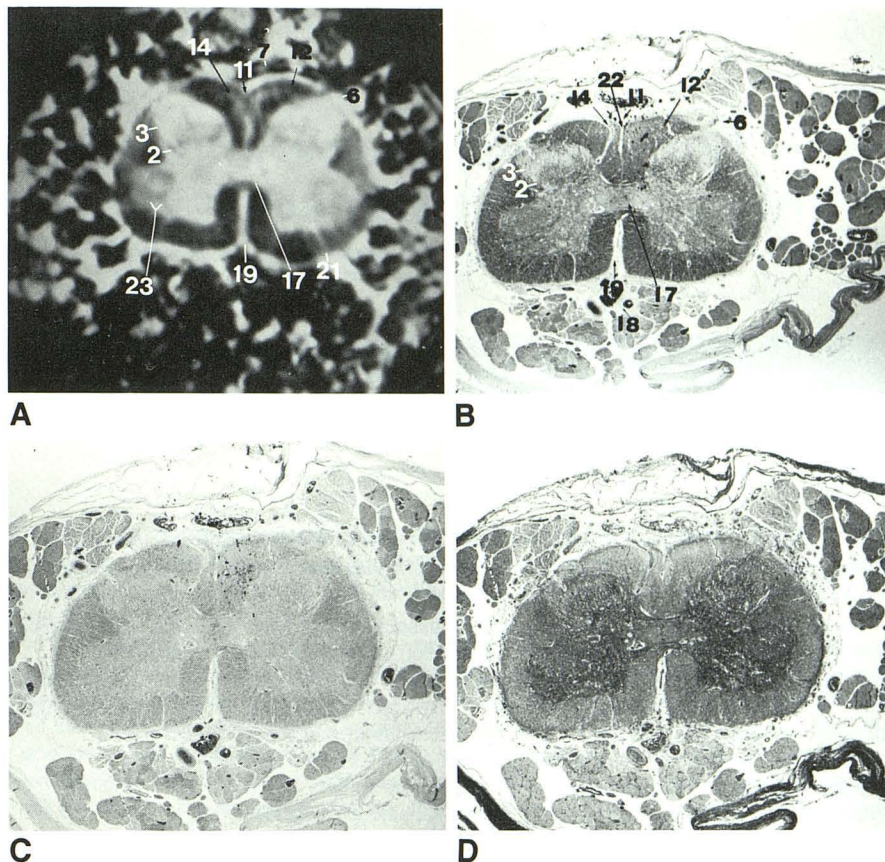
The use of small samples results in near optimization of the signal-to-noise ratio in the area of interest. Also, the appropriate loading of the RF coil can be nearly maximized. Motion, perfusion, and diffusion artifacts, which are common in *in vivo* examinations, are reduced or eliminated.

In this study we have shown that many anatomic details of human cadaveric spinal cord may be demonstrated by MR

imaging of small segments. The subarachnoid structures and topography are described. Although vascular anatomy is seen, it is not possible to differentiate venous from arterial structures without histological comparison.

Different signal intensities were observed in the gracile and cuneate fasciculi in the regions of the spinocerebellar tracts, Clarke's nucleus, and sacral cord anterior horns. Further

Fig. 5.—Sacral/cauda equina region.  
 A, MR image (800/40).  
 B, Histology section; Luxol fast blue/H and E stain.  
 C, Histology section; hematoxylin, phloxine, saffron stain.  
 D, Histology section; Bielschowsky's stain.  
 Ringlike structures (23) in anterior horns seen in MR image are not present in corresponding histology images.



histological and MR investigations are required to determine the origin and significance of these findings.

The tissue characterization achieved in this study of excised specimens is clearly beyond that of present clinical examinations. Nonetheless, the techniques and findings described here should serve as a baseline standard for subsequent clinical and in vitro examinations of the human spinal cord.

#### REFERENCES

1. Flannigan BD, Lufkin RB, McGlade C, et al. MR imaging of the cervical spine: neurovascular anatomy. *AJNR* 1987;8:27-32, *AJR* 1987;148:785-790
2. Reicher MA, Gold RH, Halbach VV, Rauschnig W, Wilson GH, Lufkin RB. MR imaging of the lumbar spine: anatomic correlations and the effects of technical variations *AJR* 1986;147:891-898
3. Hyman RA, Edwards JH, Vacirca SJ, Stein HL. 0.6 T MR imaging of the cervical spine: multislice and multiecho techniques. *AJNR* 1985;6:229-236
4. Norman D, Mills CM, Brant-Zawadzki M, Yeates A, Crooks LE, Kaufman L. Magnetic resonance imaging of the spinal cord and canal: potentials and limitations. *AJNR* 1984;5:9-14
5. Modic MT, Weinstein MA, Pavlicek W, et al. Nuclear magnetic resonance imaging of the spine. *Radiology* 1983;148:757-762
6. Carvlin MJ, Asato R, Hackney DB, Kassab E, Joseph PM. High-resolution MR of the spinal cord in humans and rats. *AJNR* 1989;10:13-17
7. Hoult DI, Richards J. The signal-to-noise ratio of the nuclear magnetic resonance experiment. *J Magn Reson* 1976;24:71-85
8. DeArmond SJ, Fusco MM, Dewey MM. *Structure of the human brain*, 2nd ed. New York: Oxford University Press, 1976:39-57
9. Carpenter MB. *Core text of neuroanatomy*, 3rd ed. Baltimore: Williams & Wilkins, 1985:52-101, 391-395
10. Daniels D, Haughton V, Naidich T. *Cervical and spinal magnetic resonance imaging: an atlas and guide*. New York: Raven Press, 1987